Solution verification of WECs: comparison of methods to estimate numerical uncertainties in the OES wave energy modelling task

Claes Eskilsson, Alex Shiri and Eirini Katsidoniotaki

Abstract—**High-fidelity models become more and more used in the wave energy sector. They offer a fully nonlinear simulation tool that in theory should encompass all linear and nonlinear forces acting on a wave energy converter (WEC). Studies using high-fidelity models are usually focusing on validation of the model. However, a validated model does not necessarily give reliable solutions. Solution verification is the methodology to estimate the numerical uncertainties related to a simulation. In this work we test four different approaches: the classical grid convergence index (GCI); a least-square version (LS-GCI); a simplified version of the least-square method (SLS-GCI); and the ITTC recommended practice. The LS-GCI requires four or more solutions whereas the other three methods only need three solutions. We apply these methods to four different high-fidelity models for the case of a heaving sphere. We evaluate the numerical uncertainties for two parameters in the time-domain and two parameters in the frequency domain. It was found that the GCI and ITTC were hard to use on the frequency domain parameters as they require monotonic convergence which sometimes does not happen due to the differences in the solutions being very small. The SLS-GCI performed almost as well as the SL-GCI method and will be further investigated.**

Index Terms—**Solution verification, validation & verification, computational fluid dynamics, wave energy**

I. Introduction

HOW to estimate the accuracy of a numerical solution when there is no exact solution to compare against? This is the question at heart of *solution verification*. Solution verification is the often overlooked part of the *verification and validation* (V&V) procedure of numerical models. The traditional verification step, in which we make sure the numerical code is working correctly by comparing to exact solutions for simplified equations, can be considered a task for code developers and thus not applicable when doing numerical analysis of wave energy converters (WECs) using established software. In the validation stage, we make sure that the underlying mathematical models approximate the application problem under investigation, typically performed by comparing numerical results to experimental test data. The vast majority of all studies of WECs using high-fidelity CFD codes have been targeting validation, see e.g. [1]–[6] to name just a few. We also refer to the review paper [7] and the numerous references within. There even exists dedicated collaborations that target the validation of numerical models for wave energy by performing blind-tests and code-to-code comparison campaigns: the Collaborative Computational Project in Wave Structure Interaction (CCP-WSI) [8]–[10] and the Ocean Energy Systems wave energy modelling task (OES-WEMT) [11]–[14]. Yet, there is another flavour of verification that is often omitted but should be performed ideally for every computational case: the solution verification. Here the uncertainty of the simulations and thus the quality of the computations are estimated.

A. Solution verification

There exists a rich literature on V&V for general CFD simulations. A good start of solution verification studies start with the classical text book of Roache [15] presenting the fundamental grid convergence index (GCI). In aeronautics there exists several standards and guidelines that dates back decades [16], [17]. With regard to the marine engineering sector the closest we have to a standard would be the International Towing Tank Conference (ITTC) recommendations [18]. However, [18] outlines the solution verification methodology but there is little discussion about what variables to actually measure convergence and uncertainty.

B. Sources of uncertainties

There are two main sources of errors and uncertainties in numerical simulations: *modelling errors* and *numerical errors*. Modelling errors arise from simplifications and approximations in the numerical model (simplified geometries, truncated computational domains, boundary conditions, turbulence models, etc.). We can divide the numerical errors into three parts [19]: (i) discretization errors (temporal and spatial errors), (ii) iterative convergence errors, and (iii) round-off errors caused by the limit of machine precision. Round-off errors can be neglected for double precision computations.

This work was supported by the Swedish Energy Agency under grant no 44423-2 and by the Danish EUDP under grant no 64020-1105.

C. Eskilsson is with the Hydrodynamic Research Unit, RISE – Research Institutes of Sweden, P.O. Box 24001, SE-400 22 Gothenburg, Sweden (e-mail: claes.eskilsson@ri.se); and the Department of the Built Environment, Aalborg University, Thomas Manns Vej 23, DK-9220 Aalborg Ø, Denmark (e-mail: claese@build.aau.dk).

A. Shiri is with the Hydrodynamic Research Unit, RISE – Research Institutes of Sweden, P.O. Box 24001, SE-400 22 Gothenburg, Sweden (e-mail: alex.shiri@ri.se).

E. Katsidoniotaki is with Division of Electricity, Uppsala University, Uppsala, Sweden; and the Centre of Natural Hazards and Disaster Science (CNDS), Uppsala, Sweden (e-mail: eirini katsidoniotaki@angstrom.uu.se).

Digital Object Identifier:
https://doi.org/10.36688/ewtec-2023-426

C. Paper contribution

There have been previous work focusing on solution verification for wave energy converters [20]–[23], and a number of studies have employed solution verification approaches to prove convergence of solutions, e.g. [24], [25]. We here present a first comparison of the uncertainties given by different solution verification approaches when applied to wave energy application. Please note that we limit the paper to only consider the *numerical spatial discretization error* and not the modelling error. However, more important is that the present paper tries to step beyond comparing response amplitude operators (RAOs), and aims to propose a set of variables to be used in solution verification of wave energy applications equally valid for decay and diffraction tests, regular waves and irregular sea states.

II. Solution verification

In the present study we will compare four different methods to estimate the numerical uncertainty:

- the original grid convergence index (GCI) method of Roache [26].
- The least-square grid convergence index (LS-GCI) method of Eça and Hoekstra and co-workers [19], [27], [28].
- a simplified variant of the least-square grid convergence index method (SLS-GCI) as presented by Tanaka and Miyake [29].
- the International Towing Tank Conference (ITTC) best practice recommendations [18], which very closely follow the work of Stern *et al.* [30].

All methods are fundamentally similar and based on (i) numerically obtained *convergence rates*, (ii) *Richardson extrapolation* to obtain estimate of the value at zero grid spacing ϕ_0, and (iii) transfer of errors to uncertainty by means of *safety factors* or *correction factors*. Nevertheless, there are subtle differences in the way the methods are devised. In the sections below we give details about the above methods, whereas Table I outlines the pros and cons of the four methods to be investigated.

TABLE I
Outline of the solution verification methods.

Method	Advantages	Disadvantages
GCI	• Only 3 meshes • Easy to implement	• Constant r • Requires monotonic convergence • Requires asymptotic convergence • Does not use standard deviation
LS-GCI	• Non-constant r • Safety factors related to convergence	• ≥ 4 meshes • Complex implementation
SLS-GCI	• Only 3 meshes • Non-constant r • Safety factors related to convergence	• Complex implementation
ITTC	• Only 3 meshes • Easy to implement • Non-constant r • Correction factors related to convergence • Avoids overly conservative safety factors	• Requires monotonic convergence

A. General definitions

We start by reminding ourselves of the difference between *error* and *uncertainty*. Error (δ) refers to the difference between a numerical solution (ϕ_i) and the exact solution (ϕ_0)

$$\delta = \phi_i - \phi_0 \,. \tag{1}$$

Uncertainty (U_{ϕ_i}) defines an interval that should contain the exact solution, i.e.,

$$\phi_i - U_{\phi_i} \leq \phi_0 \leq \phi_i + U_{\phi_i} \,. \tag{2}$$

The basis for obtaining the numerical error is grid refinement study with m grids and solutions. Let $h_1 < h_2 < \ldots < h_m$ be a sequence of meshes where h_i denotes a representative cell size and h_1 the smallest cell size. The cell size is typically obtained as

$$h_i = (N_i)^{(1/d)} \,, \tag{3}$$

where N is the element count and d is the the dimension of the mesh. The cell sizes are non-dimensionalized by dividing with h_1, i.e. $\underline{h_i} = h_i/h_1$. We further introduce the refinement ratio $r_{ij} = \underline{h_i}/\underline{h_j}$.

B. Original GCI method

The original GCI method [26] only requires two meshes, but in general three meshes are always used as the estimate for the convergence rate become highly uncertain for only 2 meshes. The sequence of meshes require a constant refinement ratio. Traditionally $r = 2$ is used, but as this can be unsustainable for larger mesh sizes $r = \sqrt{2}$ was put forward by [30]. Using three meshes the convergence rate p can be estimated as

$$p = \ln\left(\frac{\Delta_{32}}{\Delta_{21}}\right) / \ln(r) \,. \tag{4}$$

where we define $\Delta_{ij} = \phi_i - \phi_j$. By using Richardson extrapolation we can estimate the converged value ϕ_0

$$\phi_0 \approx \phi_1 + \frac{\phi_1 - \phi_2}{r^p - 1} \,, \tag{5}$$

and thus the error

$$\delta^1_{RE} = \phi_1 - \phi_0 = \frac{\Delta_{21}}{r^p - 1} \,. \tag{6}$$

A key step in [26] is that the numerical errors are converted into uncertainties by means of safety factors F_S, giving

$$U_\phi = F_S \left|\delta\right| \,. \tag{7}$$

In the original GCI method we require the convergence to be asymptotic ($0.95 \leq p \leq 2.05$, for a standard second-order scheme) and the safety factors are simply set to 1.25 if three or more meshes are used and 3.0 if only two meshes are used.

Thus we get the following two expressions of the uncertainty, one for the finest resolution

$$U_1 = \frac{1.25|\Delta_{21}|}{r^p - 1}, \tag{8}$$

and one for the coarser resolution

$$U_2 = \frac{1.25|\Delta_{21}|r^p}{r^p - 1}. \tag{9}$$

C. Least-square GCI method

A more refined GCI approach is due to Eça and Hoekstra and co-workers [19], [27] using a least-square approach.

The numerical error is estimated as

$$\delta_{RE} = \phi_i - \phi_0 = a\underline{h}_i^p, \tag{10}$$

in which p is the numerically obtained order of convergence and a is a case specific constant. Assuming first and second order convergence as well as a mixture of first and second order convergence we additionally have

$$\delta_{RE}^{01} = \phi_i - \phi_0 = a_{01}\underline{h}_i^1, \tag{11}$$
$$\delta_{RE}^{02} = \phi_i - \phi_0 = a_{02}\underline{h}_i^2, \tag{12}$$
$$\delta_{RE}^{12} = \phi_i - \phi_0 = a_{11}h_i^1 + a_{12}\underline{h}_i^2. \tag{13}$$

Using a least square approach we then evaluate ϕ_0, p as well as the constants to obtain the errors.

Following [26], the numerical errors are converted into uncertainties by means of safety factors. Here, however, the values of the applied safety factors follow from the convergence. If $p > 0$ the convergence is monotone, otherwise it is oscillatory. If in addition the convergence is in the asymptotic range ($0.95 \leq p \leq 2.05$) the safety factor is set to 1.25. If the convergence is monotonic but not in the asymptotic range, then the safety factor is set to 3.

In addition, the uncertainties are not only directly following the computed errors but are also dependent on the standard deviations. Thus, the larger the mesh sequence, the more improved the estimated uncertainties become. To summarize, the uncertainties can be evaluated as

$$U_\phi = 1.25\delta_{RE} + U_S \qquad \text{if } p \in [0.95,\, 2.05], \tag{14}$$
$$U_\phi = \min\left(1.25\delta_{RE} + U_S,\, 3\delta_{RE}^{12} + U_S^{12}\right) \text{ if } p < 0.95, \tag{15}$$
$$U_\phi = \max\left(1.25\delta_{RE} + U_S,\, 3\delta_{RE}^{02} + U_S^{02}\right) \text{if } p > 2.05, \tag{16}$$

where U_S, U_S^{02} and U_S^{12} are the standard deviations obtained from the least square fits. In the case of oscillatory convergence, a range-based estimate is employed

$$U_\phi = 3\delta_{\Delta M}, \tag{17}$$

in which the error between the maximum and minimum is obtained as

$$\delta_{\Delta M} = \frac{\max|\phi_i - \phi_j|}{(h_m/h_1) - 1} \qquad 1 \leq i, j \leq m. \tag{18}$$

D. Simplified least-square GCI method

As in the LS-GCI method the exact value, the convergence rate and the constants are obtained using least-squares. This version is alleged to work with only three meshes. Upper (p_u) and lower (p_l) thresholds of the convergence of the discretization schemes are introduced. In this work we set the lower threshold to $p_l = 0.95$ and the upper threshold to $p_u = 2.05$, as we are working with second order discretrization schemes and in order to harmonize with the LS-GCI method.

The uncertainties are then evaluated as

$$U_\phi = 1.25\delta_{RE} + U_S \qquad \text{if } p \in [0.95,\, 2.05], \tag{19}$$
$$U_\phi = 3\delta_{RE}^{01} + U_S^{01} \qquad \text{if } p \in (0,\, 0.95), \tag{20}$$
$$U_\phi = 3\delta_{RE} + U_S \qquad \text{if } p > 2.05. \tag{21}$$

For the case of oscillatory or not converged solutions ($p < 0$) we compute the uncertainty as

$$U_\phi = U_S^m = \sqrt{\frac{1}{3}\sum_{k=1}^{3}\left(\phi_k - \bar{\phi}\right)^2}, \tag{22}$$

where $\bar{\phi}$ denotes the mean of ϕ.

E. ITTC

The ITTC guidelines [18] lean heavily upon the work of Stern and co-workers [30], in which uncertainty estimates are obtained using *correction factors* rather than safety factors. Stern *et al.* argues that the safety factor approach can be overly conservative.

The approach requires only $m = 3$ solutions, albeit $m = 5$ is required if higher-order terms are sought after. In this work we use $m = 3$. If r is constant then (4) can be used. If r is not constant the convergence is estimated by

$$p = \frac{\ln\left(\Delta_{32}/\Delta_{21}\right)}{\ln(r_{21})} + \frac{1}{\ln(r_{21})}\left(\ln(r_{32}^p - 1) - \ln(r_{21}^p - 1)\right). \tag{23}$$

The error is now estimated by (6) multiplied with a correction factor F_C, giving

$$\delta_{RE}^* = F_C\,\delta_{RE}^1 = F_C\,\frac{\Delta_{21}}{r^p - 1}. \tag{24}$$

The correction factor can be estimated as

$$F_C = \frac{r^p - 1}{r^{p_{est}} - 1}. \tag{25}$$

Here p_{est} is an estimate for the limiting orders of accuracy in the asymptotic range. In this work we use the theoretical order of accuracy $p_{est} = 2$.

The uncertainty is given by bounding the error by the sum of the absolute value of the correction and the absolute value of the amount of correction

$$U_\phi = \left(|F_C| + |1 - F_C|\right)|\delta_{RE}^1|. \tag{26}$$

TABLE II
NUMERICAL MODELS USED.

Label	Code	Main features
RANS1	OpenFOAM-v2212	Incompressible RANS, FVM, implicit timestepping, algebraic VOF , mesh morphing
RANS2	OpenFOAM-v2212	Incompressible RANS, FVM, implicit timestepping, geometric VOF, mesh morphing
RANS3	OpenFOAM-v1912	Incompressible RANS, FVM, implicit timestepping, algebraic VOF, overset mesh
FNPF1	Shipflow MOTIONS-v7	FNPF, BEM, explicit timestepping, MEL

There are several versions of expressions with regard to uncertainty and correction factors. ITTC [18] lists the one given by Wilson *et al.* [31] as recommended:

$$U_\phi = \left(2.4\left(1-F_C\right)^2 + 0.1\right)\left|\delta^1_{RE}\right| \quad \text{if } |1-F_C| < 0.125\,, \tag{27}$$

$$U_\phi = \left(1-F_C\right)\left|\delta^1_{RE}\right| \quad \text{if } |1-F_C| \geq 0.125\,. \tag{28}$$

III. PARAMETERS

Of paramount importance for the usability of the solution verification is for which parameters we estimate the numerical uncertainty. Typically the parameters are expressed in non-dimensional form. This is easily achievable: using RAOs for responses and any forces can be non-dimensionalized with e.g. the hydrostatic stiffness. In this study we will use decay coefficient (c) and decay period (T_r) for decay tests and RAOs ($\hat{x}$) and response period (T_r) for analyses in the time-domain. The periods are non-dimensionalized with the analytical damped natural period.

However, in order to device a metric usable for all cases, regular as well as irregular, we will look into the results in spectral form and look at the convergence of the spectral moments and variables derived from the spectral moments. Thus, we will compare traditional parameters based for convergence like RAO and decay coefficients to their spectral moments. We define the spectral moments as

$$m_n = \int_0^\infty f^n F(f)\mathrm{d}f \tag{29}$$

where f is the frequency and F is a function. Especially, we will look into the convergence of the variance $\sigma = \sqrt{m_0}$ and the response period given by $T_{02} = \sqrt{m_0/m_2}$.

IV. NUMERICAL MODELS

In contrast to the previous work [12] and [13], this study is restricted to the use of high-fidelity models, i.e., unsteady RANS and FNPF models. For high-fidelity models numerical discretization errors are important and thus we can use solution verification procedures developed for general CFD. For LPF/WNPF models modelling errors can be expected to be significantly larger than the numerical discretization errors. Thus the benefit of performing the solution verification approaches discussed in section II for LPF/WNPF models would be limited, and they are thus not included in the study.

The four different numerical models used and their main features are presented in Table II. Out of the four models, two are versions of the Reynold-averaged Navier-Stokes (RANS) multi-phase `interFoam` solver in the `OpenFOAM` open-source framework founded on the cell-centred finite volume method (FVM) [32], [33].

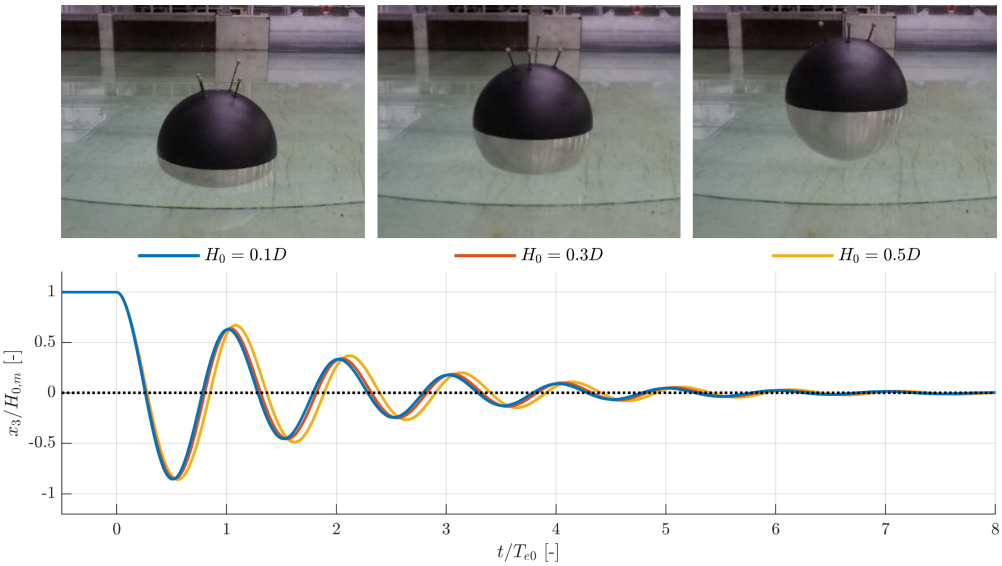

Fig. 1. Decay tests of a sphere. Top: Photos of the sphere at the initial positions for the three drop cases. Bottom: Normalised time series of recorded heave motion for the three drop height. From [13].

TABLE III
SPHERE DATA. FROM [13].

Parameter	Unit	Value
Diameter (D)	m	0.300
Mass (m)	kg	7.056
Center of gravity (CoG)	m	(0, 0, -0.0348)
Roll moment of inertia (I_{xx})	kgm^2	0.098251
Pitch moment of inertia (I_{yy})	kgm^2	0.098254
Yaw moment of inertia (I_{zz})	kgm^2	0.073052
Water depth (d)	m	0.9
Acceleration of gravity (g)	ms^{-2}	9.82
Water density (ρ_w)	kgm^{-3}	998.2

Another is a version of the `interIsoFoam` solver also available in `OpenFOAM`. The main difference between these two solvers are the use of algebraic vs geometric volume of fluid (VOF) implementations. `interFoam` relies on the so-called multidimensional universal limiter for explicit solution (MULES) and an interface compression scheme. In contrast, `interIsoFoam` relies on the geometric VOF called isoAdvector as presented in [34]. IsoAdvector reconstructs the interface inside the cells using an isosurface concept. Additionally, we use two different mesh motion strategies inside `OpenFOAM`: the classical mesh morphing approach and the overset mesh where a separate body mesh moves on top of a background mesh.

The last model solves the fully nonlinear potential flow (FNPF) equations, i.e. the Laplace equation together with the fully nonlinear free surface conditions. The FNPF model used is the Shipflow-Motions 7 [35], [36]. The FNPF equations are solved using an unsteady three-dimensional boundary element method (BEM) together with a mixed Eulerian–Lagrangian method (MEL) for the free surface. The BEM model is a surface model, with panels om the body and free surface (and also on the bottom for finite depth cases). In contrast to the FVM volume methods, the BEM surface method uses significantly less degrees of freedom to handle the problems.

V. TEST CASES

We use the fundamental case of a heaving sphere for this work. The heaving sphere was initially investigated in full-scale (with a sphere diameter of D=10 m) as the first test case of the OES-WEMT [12]. Decay, regular waves and irregular wave cases, with different power take-off (PTO) damping coefficients, were investigated in [12], [37]. The decay test was later re-visited in model-scale (D=0.3m) in Kramer *et al.* [13]. Kramer *et al.* performed an highly-accurate experimental campaign, with an experimental uncertainty below 0.3 % in response amplitude, see Fig. 1. In this work we use the model-scale set-up [13], with Froude-scaled settings taken from [12] where needed.

The experimental campaign was carried out in the wave basin at Aalborg University, Denmark. The wave tank is 13.00×8.44m with 0.9m water depth. The origin of the global coordinate system is located in the middle of the basin with z-axis pointing upwards from the still free surface elevation. The origin of the body local coordinate system is located at the center of the sphere; and coincide with the global coordinate system when the sphere is at equilibrium. The sphere is defined in Table III. As the sphere is restricted to move in heave only, there is no mooring defined for the sphere cases.

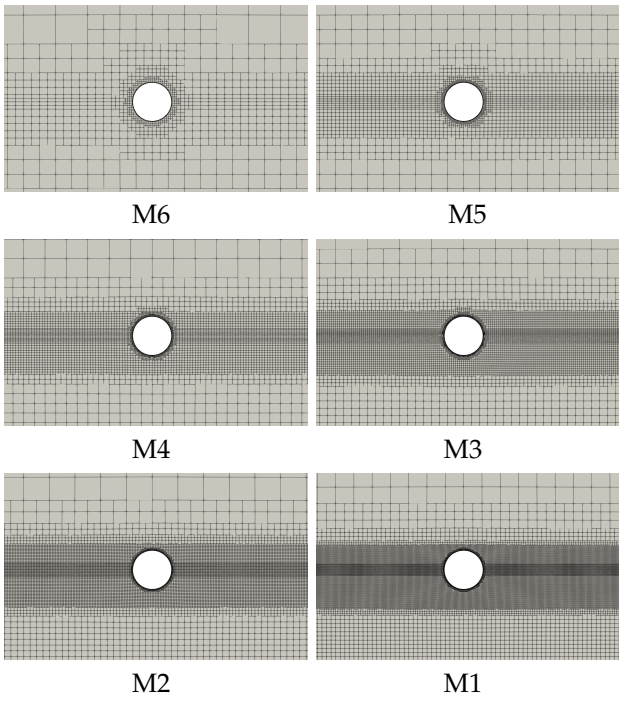

Fig. 2. Example of the mesh sequence used for the RANS1 and RANS2 models.

A. Mesh sequences

The choice of mesh sequence greatly affects the later analyses. Here we use sequences made up of six meshes designed so a subsection of the meshes give rise to a three mesh sequence with constant refinement ratio, as required by the CGI method. Fig. 2 shows the meshes used for the RANS1 and RANS2 models. The meshes have been uniformly refined by changing the underlying base resolution and keeping the refinement levels defined by the refinement boxes equal for all meshes. The resulting number of cells are $N = [9.91, 3.79, 2.00, 0.87, 0.28, 0.05]$ million cells.

The RANS3 model uses overset meshes with mesh sizes of $h = [0.06, 0.03, 0.021, 0.015, 0.011, 0.0075]$ m with refinement zones around the free surface.

The FNPF1 model uses the same panel number for the free surface ($\approx$ 4000) with refinement around the body. The body mesh is refined as: $N = [500, 1125, 2000, 3125, 4500, 6125]$ panels.

For all numerical models we will denote the most dense mesh with M1, the second most dense mesh with M2, and so on to the coarsest mesh being denoted with M6.

B. Heave decay of a sphere

Three drop heights (H_0) were considered in the experiments: $H_0 = [0.1D, 0.3D, 0.5D]$. The largest drop height equals the sphere just being lifted out of the

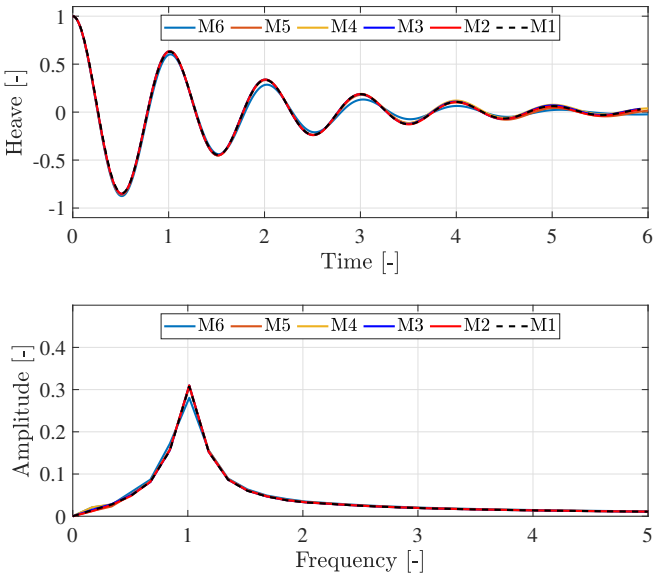

Fig. 3. Heave decay of a sphere with $0.1D$ drop height for different mesh resolutions for model RANS1. Top panel: time series and bottom panel: frequency domain.

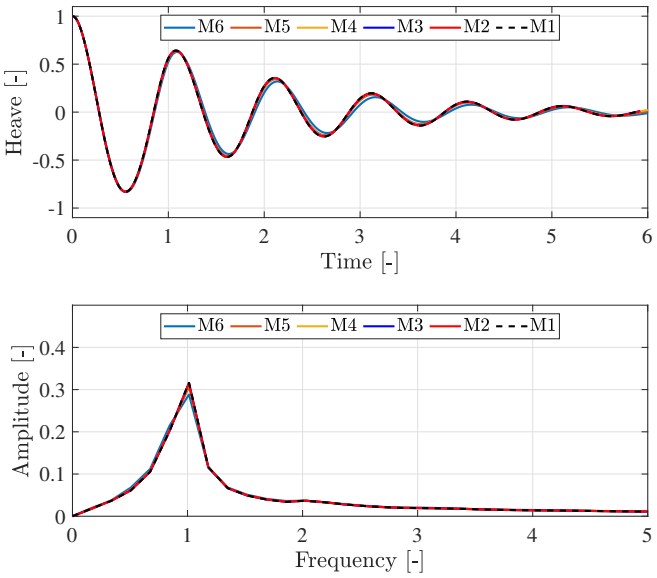

Fig. 4. Heave decay of a sphere with $0.5D$ drop height for different mesh resolutions for model RANS1. Top panel: time series and bottom panel: frequency domain.

water, see Fig. 1. The analytical damped natural period is $T_{e0} = 0.76$ s [13]. From the experimentally recorded non-dimensional response in Fig. 1 we see that not much differs between the $0.1D$ and $0.3D$ cases. Thus we only consider the $0.1D$ and $0.5D$ cases in the numerical analysis.

Figs. 3 and 4 show the results in time- and spectral domain using the RANS1 model. From visual inspection it appears only the most coarse mesh gives different solutions, the lines appear to be on top of each other. We also see that the spectrum gets wider. Even in the decay tests there are multiple frequencies active. For the $0.5D$ case there is a pronounced skewness to the spectrum.

C. Heaving sphere in regular waves

This section uses a Froude scaled setting of the cases modelled with LPF/WNPK in [12]. The model-scale is $\lambda = 1/33.33$. We choose the settings that yields the largest heave response according to [12]: an incident Stokes V wave at the resonance period $T_{e0} = 0.76$ s with wave steepness $H/L = 0.0628$ ($H = 0.05845$ m and $L = 0.9317$ m) and no PTO damping.

Fig. 5 shows the results in time- and spectral domain using the RANS1 model. In contrast to the previous test case, here we see a more standard convergence with the heave amplitude growing with increasing mesh size.

VI. Uncertainty results

We use the LS-GCI results as a baseline as they are performed using the largest mesh sequence. Thus, we will present those results in some detail and then compare the results from the other methods to the LS-GCI results.

A. Heave decay of a sphere

We start by comparing the different numerical models behavior using the LS-GCI method. The results are shown in Fig. 6. The immediate results is that the results from the RANS3 model is associated with larger uncertainties than the other three models. This highlights the difficulty in defining an overset mesh and that overset meshes can have larger uncertainties than more standard mesh-morphing approaches. We also see that the RANS1 model exhits somewhat larger uncertainties than the RANS2 model especially for the coarser meshes. The RANS2 model provides excellent results for coarse meshes for the smaller motion $0.1D$ case. The FNPF1, with regard to uncertainties, give very good results already for the M5 mesh as it is only M6 that shows a larger uncertainty than the 5% rule-of-thumb. This is partially due to the fact that it is only the body mesh that changes, while the surface mesh is already well resolved even for the M6 mesh.

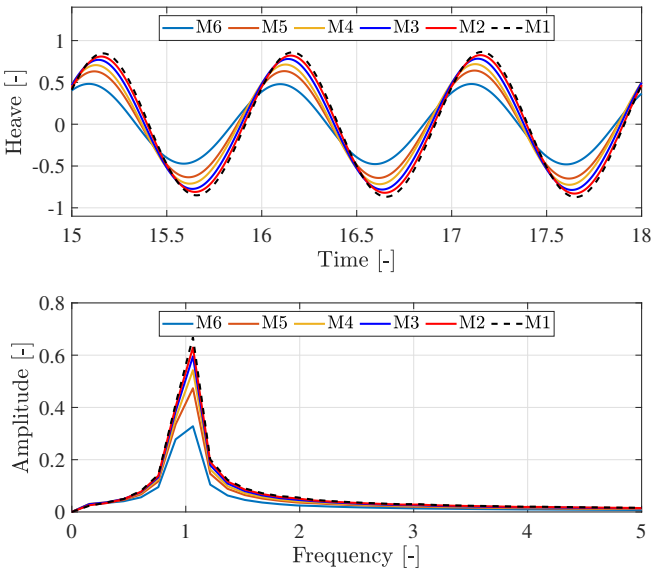

Fig. 5. Heave motion of a sphere in regular waves for different mesh resolutions for model RANS1. Top panel: time series and bottom panel: frequency domain.

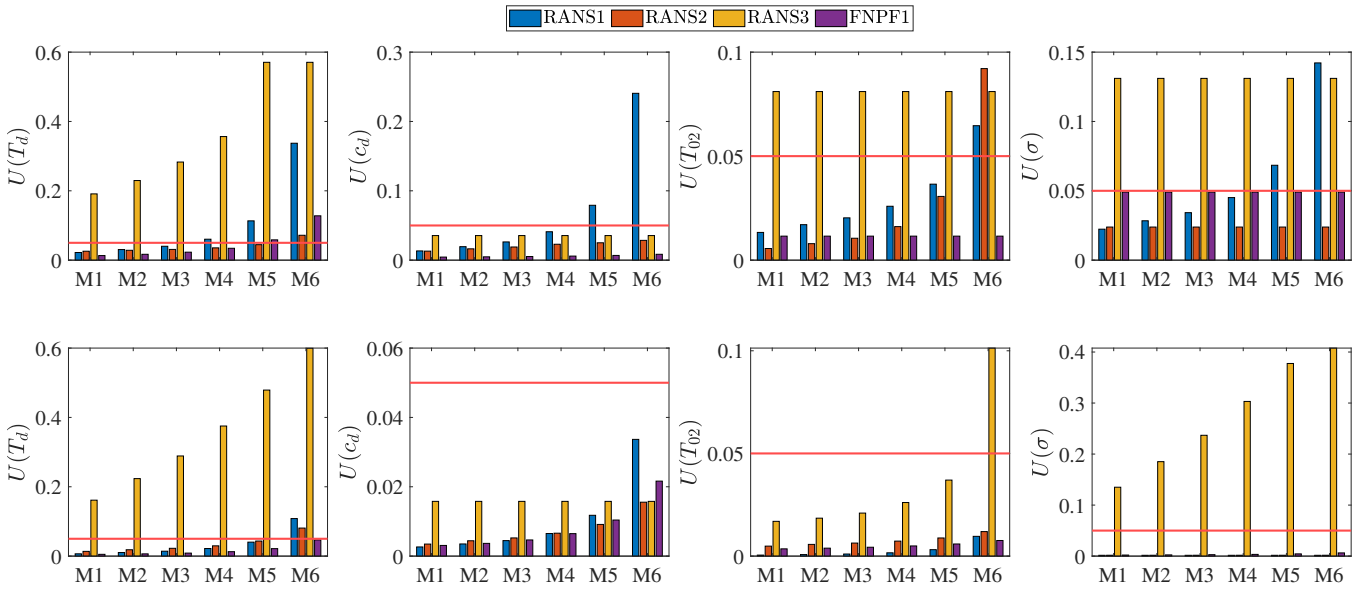

Fig. 6. Heave decay of a sphere with 0.1 drop height (top panel) and $0.5D$ drop height (bottom panel). Uncertainties for different mesh resolutions for different models using LS-GCI. The solid red lines show the 5% uncertainty.

Comparing the uncertainties of the time-domain variables to the frequency domain variables, there is a general agreement. If the time-domain solutions have a $U < 0.05$ then most likely also the frequency domain solutions will have a low uncertainty. There were more instances of non-monotonically converged solutions for the frequency domain variables. These instances were mostly due to the error being so small it became unstable to compute the least-squares. However, U still became small as the range-based estimate (17) was small since the differences in ϕ_i were minute.

Clearly, the $0.1D$ case is more difficult to resolve with low uncertainty. From Fig. 6, we would conclude that RANS1 model would need to use the M3 and M5 meshes for the $0.1D$ and $0.5D$ cases, respectively. The RANS2 model would manage with the M5 mesh for both cases, whereas the FNPF1 model need M5 for $0.1D$ but can use the coarsest M6 mesh for the $0.5D$ case. The RANS3 model is yet not fully converged. However, it is more interesting to look at the accuracy of the solutions versus the computational cost. Fig. 7 shows the uncertainty versus computational cost in CPU hours. We see that the FNPF1 models are surprisingly heavy, we would expect the FNPF to be at least an order of magnitude faster [3]. This is of course due to using a fixed resolution of the free surface that gives a larger than necessary overhead. It can alse be seen that even though the RANS2 model is more accurate per resolution than RANS1, it is also more computational costly, so the 'accuracy per CPU hour' becomes more similar for the $0.5D$ case. For small motions the RANS2 method is still to be recommended.

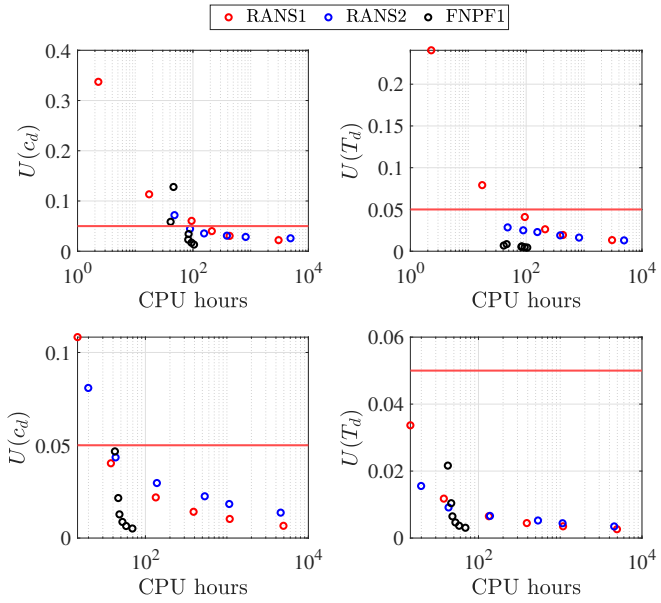

Fig. 7. Heave decay of a sphere with 0.1 drop height (top panel) and $0.5D$ drop height (bottom panel). Uncertainties for different mesh resolutions for different models using LS-CGI versus computational effort. The solid red lines show the 5% uncertainty.

We use the M6, M5 and M3 meshes for comparing the LS-GCI computed uncertainties to the original GCI, SLS-GCI and the ITTC approaches. We present the uncertainties obtained by the different methods for RANS1 model with the M3 mesh in Table IV. The original GCI and ITTC methods fails for non-monotonically converging cases, indicated by the dashes in the table. This is a significant shortcoming since the frequency

TABLE IV
UNCERTAINTIES FOR THE DECAY TEST USING DIFFERENT METHODS.

Case	Parameter	LS-GCI	SLS-GCI	GCI	ITTC
$0.1D$	$U(T_d)$	4.00E-02	6.30E-04	3.76E-04	2.49E-04
	$U(c_d)$	2.62E-02	2.40E-03	1.35E-03	6.36E-04
	$U(T_{02})$	2.03E-02	4.66E-02	—	—
	$U(\sigma)$	3.42E-02	1.12E-01	—	—
$0.5D$	$U(T_d)$	1.42E-02	1.88E-02	2.48E-02	1.18E-02
	$U(c_d)$	4.47E-03	7.41E-03	9.87E-03	5.26E-03
	$U(T_{02})$	1.02E-03	1.12E-04	6.26E-05	2.69E-05
	$U(\sigma)$	1.60E-03	1.07E-03	—	—

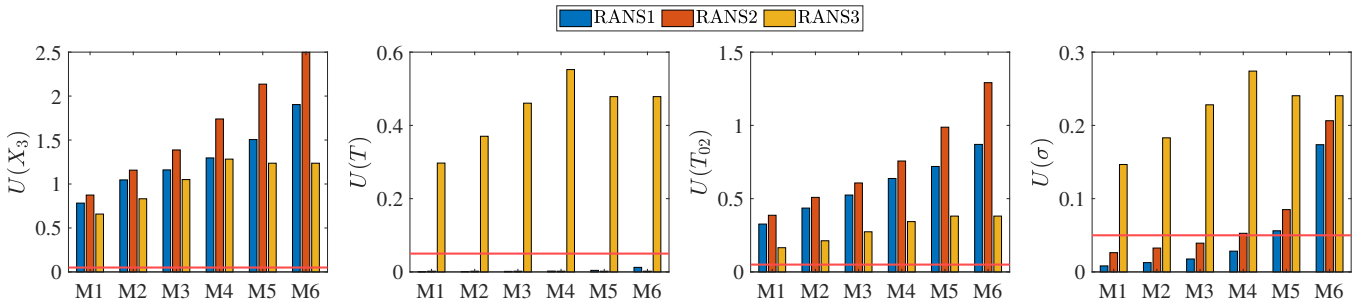

Fig. 8. Heave of a sphere in regular waves. Uncertainties for different mesh resolutions for different models using LS-GCI. The solid red lines show the 5% uncertainty.

based parameters only exhibits oscillatory convergence due to values being very close. The least square methods naturally handles this situation. Otherwise the simpler three mesh methods provide good estimated compared to the six mesh LS-GCI method. For the $0.5D$ case the time-domain uncertainties are very similar, whereas for the $0.1D$ case the uncertainties are somewhat under-predicted.

B. Heaving sphere in regular waves

We repeat the above exercise for the case of a regular wave. The time-series and spectrum presented in Fig. 5 are processed using the LS-GCI method for the time-domain variables of heave RAO (X_3) and response period (T), as well as for the variance of the spectrum ($\sigma = \sqrt{m_0}$) and the spectral response period ($T_{02} = \sqrt{m_0/m_2}$). The resulting uncertainties are presented in Fig. 8. This is a significantly harder case than the decay tests, and clearly none of the models are even close to be numerically converged. This is in stark contrast to the outcome of a more traditional grid convergence study done by plotting the solutions like in Fig. 5. From Fig. 5 it would be tempting to state that M1 is indeed a grid independent solution, but the results in Fig. 8 clearly show how wrong such as conclusion would be. This case requires significantly denser meshes to yield reliable solutions.

VII. Conclusion

The reliability of a numerical solution can be judged by means of V&V methodologies and solution verification should be carried out on a regular basis. There are many versions of solution verification approaches, we have used the least-square grid convergence index (LS-GCI) method [19] as our baseline method. The LS-GCI method is the most flexible, but also the most computationally costly method (more than four meshes) and it can be a bit complex to implement. Nevertheless, there exist freely available tools, e.g. the toolbox [38] from Marin comes highly recommended. Of the methods that only rely on three meshes the original GCI and ITTC methods fails for non-monotonically converging cases which is a significant shortcoming. The simplified LS-GCI method [29] appears to match the LS-GCI method for the decay cases and will be further tested.

A comparison between standard time-domain parameters and spectral parameters based on straightforward spectral moments was initiated. However, the present study just started looking into this issue and the investigation to find the best choice of parameters is far from finished. To standardise the metric used when estimating the numerical uncertainty of high-fidelity modelling of WECs would allow for easier evaluations of the results. A spectral moment based metric is independent of whether we are dealing with a decay, diffraction, regular or irregular wave case. The results in this study indicate that it might be feasible route, albeit it is a significant short coming of the study that no irregular waves were studied. This is on-going work but running full irregular sea-states in CFD is highly time-consuming.

Finally, to define and implement standardized methods to express the confidence in numerical simulations of WECs are of utmost importance. Today, there is no guidelines specific for WECs, the closest would be the recommendations of ITTC [18]. The present study was initiated within the Ocean Energy Systems wave energy modelling task, and we hope this work will continue in that project.

Acknowledgement

We gratefully acknowledge that the computations were performed on resources at the National Supercomputer Centre provided by the National Academic Infrastructure for Supercomputing in Sweden (NAISS).

References

[1] P. Schmitt and B. Elsaesser, "On the use of OpenFOAM to model oscillating wave surge converters," *Ocean Engineering*, vol. 108, pp. 98–104, 2015. [Online]. Available: https://www.sciencedirect.com/science/article/pii/S0029801815003686

[2] J. Palm, C. Eskilsson, G. M. Paredes, and L. Bergdahl, "Coupled mooring analysis for floating wave energy converters using CFD: Formulation and validation," *International Journal of Marine Energy*, vol. 16, pp. 83–99, 2016.

[3] E. Ransley, D. Greaves, A. Raby, D. Simmonds, and M. Hann, "Survivability of wave energy converters using CFD," *Renewable Energy*, vol. 109, pp. 235–247, 2017. [Online]. Available: https://www.sciencedirect.com/science/article/pii/S0960148117301799

[4] I. Simonetti, L. Cappietti, H. Elsafti, and H. Oumeraci, "Evaluation of air compressibility effects on the performance of fixed OWC wave energy converters using CFD modelling," *Renewable Energy*, vol. 119, pp. 741–753, 2018. [Online]. Available: https://www.sciencedirect.com/science/article/pii/S0960148117312235

[5] C. Windt, N. Faedo, D. García-Violini, Y. Peña-Sanchez, J. Davidson, F. Ferri, and J. V. Ringwood, "Validation of a CFD-based numerical wave tank model of the 1/20th scale Wavestar wave energy converter," *Fluids*, vol. 5, no. 3, 2020. [Online]. Available: https://www.mdpi.com/2311-5521/5/3/112

[6] E. Katsidoniotaki, Z. Shahroozi, C. Eskilsson, J. Palm, J. Engström, and M. Göteman, "Validation of a CFD model for wave energy system dynamics in extreme waves," *Ocean Engineering*, vol. 268, p. 113320, 2023. [Online]. Available: https://www.sciencedirect.com/science/article/pii/S0029801822026038

[7] C. Windt, J. Davidson, and J. V. Ringwood, "High-fidelity numerical modelling of ocean wave energy systems: A review of computational fluid dynamics-based numerical wave tanks," *Renewable and Sustainable Energy Reviews*, vol. 93, pp. 610–630, 2018. [Online]. Available: https://www.sciencedirect.com/science/article/pii/S1364032118303629

[8] "https://ccp-wsi.ac.uk," 2023.

[9] E. Ransley *et al.*, "Numerical simulation of focused wave interactions with a fixed FPSO-like structure - a comparative study: Results from the CCP-WSI blind test series 1," *International Journal of Offshore and Polar Engineering*, vol. 29, no. 2, pp. 28–137, 2019.

[10] E. J. Ransley *et al.*, "Focused wave interactions with floating structures: a blind comparative study," *Proceedings of the Institution of Civil Engineers - Engineering and Computational Mechanics*, vol. 174, no. 1, pp. 46–61, 2021. [Online]. Available: https://doi.org/10.1680/jencm.20.00006

[11] "https://www.ocean-energy-systems.org/oes-projects/wave-energy-converters-modelling-verification-and-validation/," 2023.

[12] F. Wendt *et al.*, "Ocean energy systems wave energy modelling task: Modelling, verification and validation of wave energy converters," *Journal of Marine Science and Engineering*, vol. 7, no. 11, 2019. [Online]. Available: https://www.mdpi.com/2077-1312/7/11/379

[13] M. B. Kramer *et al.*, "Highly accurate experimental heave decay tests with a floating sphere: A public benchmark dataset for model validation of fluid–structure interaction," *Energies*, vol. 14, no. 2, 2021. [Online]. Available: https://www.mdpi.com/1996-1073/14/2/269

[14] H. B. Bingham *et al.*, "Ocean Energy Systems wave energy modeling task 10.4: Numerical modeling of a fixed oscillating water column," *Energies*, vol. 14, no. 6, 2021. [Online]. Available: https://www.mdpi.com/1996-1073/14/6/1718

[15] P. J. Roache, *Fundamentals of Verification and Validation*. Albuquerque, NM: Hermosa Publishers, 2009.

[16] AIAA, "Guide for verification and validation of computational fluid dynamics simulations," *AIAA Standards*, no. AIAA G-077-1998, 1998.

[17] ASME, "Standard for Verification and Validation in Computational Fluid Dynamics and Heat Transfer," American Society of Mechanical Engineers, Standard No. V V20, 2009.

[18] ITTC, "ITTC Quality Manual, Uncertainty Analysis in CFD," International Towing Tank Conference, Recommended Procedures and Guidelines, 2017.

[19] L. Eça and M. Hoekstra, "A procedure for the estimation of the numerical uncertainty of CFD calculations based on grid refinement studies," *Journal of Computational Physics*, vol. 262, pp. 104 – 130, 2014.

[20] C. Eskilsson, J. Palm, and L. Bergdahl, "On numerical uncertainty of VOF-RANS simulations of wave energy converters through V&V techniques," in *Proceedings of the 12th European Wave and Tidal Energy Conference (EWTEC2017)*, Cork, Ireland, 2017.

[21] W. Wang, M. Wu, J. Palm, and C. Eskilsson, "Estimation of numerical uncertainty in CFD simulations of a passively controlled wave energy converter," *Proceedings of the Institution of Mechanical Engineers, Part M: Journal of Engineering for the Maritime Environment*, vol. 232, no. 1, pp. 71–84, 2018.

[22] S. A. Brown, E. J. Ransley, P.-H. Musiedlak, and D. Greaves, "Quantifying the Predictive Capability of OpenFOAM 5.0: Focused Wave Impacts with Floating Bodies," *International Journal of Offshore and Polar Engineering*, vol. 30, no. 01, pp. 20–27, 03 2020. [Online]. Available: https://doi.org/10.17736/ijope.2020.jc779

[23] T. Amaral, M. Rentschler, G. Vaz, and J. Baltazar, "Comprehensive Verification and Validation of a CFD Analysis," ser. International Conference on Offshore Mechanics and Arctic Engineering, vol. Volume 8: Ocean Renewable Energy, 06 2022, v008T09A072. [Online]. Available: https://doi.org/10.1115/OMAE2022-80578

[24] C. Windt, J. Davidson, P. Schmitt, and J. V. Ringwood, "Wave–structure interaction of wave energy converters: a sensitivity analysis," *Proceedings of the Institution of Civil Engineers - Engineering and Computational Mechanics*, vol. 173, no. 3, pp. 144–158, 2020. [Online]. Available: https://doi.org/10.1680/jencm.19.00033

[25] E. Katsidoniotaki and M. Göteman, "Numerical modeling of extreme wave interaction with point-absorber using OpenFOAM," *Ocean Engineering*, vol. 245, p. 110268, 2022. [Online]. Available: https://www.sciencedirect.com/science/article/pii/S0029801821015754

[26] P. J. Roache, "Quantification of uncertainty in computational fluid dynamics," *Annual Review of Fluid Mechanics*, vol. 29, pp. 123–160, 1997.

[27] L. Eça, G. Vaz, and M. Hoekstra, "A verification and validation exercise for the flow over a backward facing step," in *Fifth European Conference on Computational Fluid Dynamics*, 14-17 June Lisbon, Portugal, 2010.

[28] L. Eça, G. Vaz, S. L. Toxopeus, and M. Hoekstra, "Numerical Errors in Unsteady Flow Simulations," *Journal of Verification, Validation and Uncertainty Quantification*, vol. 4, no. 2, 07 2019, 021001. [Online]. Available: https://doi.org/10.1115/1.4043975

[29] M. Tanaka and Y. Miyake, "Numerical simulation of thermal striping phenomena in a T-junction piping system for fundamental validation and uncertainty quantification by GCI estimation," *Mechanical Engineering Journal*, vol. 2, no. 5, pp. 15–00 134, 2015.

[30] F. Stern, R. V. Wilson, H. W. Coleman, and E. G. Paterson, "Comprehensive approach to verification and validation of CFD simulations – Part 1: Methodology and procedures," *Journal of Fluids Engineering*, vol. 123, pp. 793–802, 2001.

[31] R. Wilson, J. Shao, and F. Stern, "Discussion: Criticisms of the "Correction Factor" Verification Method 1," *Journal of Fluids Engineering*, vol. 126, no. 4, pp. 704–706, 09 2004. [Online]. Available: https://doi.org/10.1115/1.1780171

[32] "www.openfoam.com," 2023.

[33] H. Weller, G. Tabor, H. Jasak, and C. Fureby, "A tensorial approach to computational continuum mechanics using object-oriented techniques," *Computers in Physics*, vol. 12, no. 6, pp. 620–631, 1998.

[34] J. Roenby, H. Bredmose, and H. Jasak, "A computational method for sharp interface advection," *R. Soc. open sci.*, vol. 3, pp. 160 405–160 405, 2016.

[35] Flowtec, "http://www.flowtec.se," 2022.

[36] M. Kjellberg, "Fully nonlinear unsteady three-dimensional boundary element method for ship motions in waves," Ph.D. dissertation, Chalmers University of Technology, 2013.

[37] F. Wendt *et al.*, "International energy agency ocean energy systems task 10 wave energy converter modeling verification and validation," in *Proceedings of the 12th European Wave and Tidal Energy Conference*, Cork, Ireland, 2017.

[38] "https://www.marin.nl/en/research/free-resources/verification-and-validation/verification-tools," 2023.